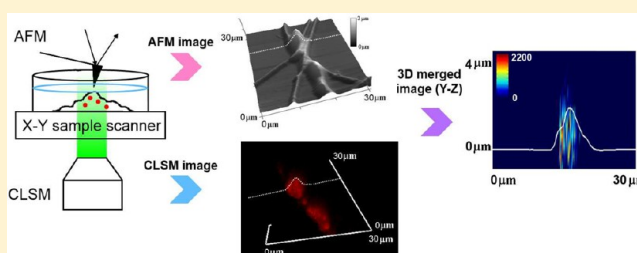


Presynaptic Structure of *Aplysia* Single Live Neuron by Atomic Force and Confocal Laser Scanning Microscope

Aee-Young Park,[†] Yeon-Su Chae,[‡] Seung-Hee Lee,[‡] Bong-Kiun Kaang,^{*,‡} and Seonghoon Lee^{*,†}

[†]Molecular Electronics and NanoStructures Laboratory, School of Chemistry, NS60, and [‡]National Creative Research Initiative Center for Memory, Department of Biological Sciences, College of Natural Sciences, Seoul National University, Seoul 151-747, Republic of Korea

ABSTRACT: The structural and functional plasticity of *Aplysia* mechanosensory presynaptic neurons has been studied in relation with the mechanism underlying learning and memory. Long-term facilitation (LTF), which is a well-known cellular model for long-term memory in *Aplysia*, is accompanied by new synaptic structural growth or change. We developed a combined atomic force microscope and confocal laser scanning microscope (AFM-CLSM) system integrated with a MATLAB routine for image processing to concurrently obtain high-resolution 3-dimensional (3D) outer-surface morphological images and 3D interior fluorescence images. With our combined AFM-CLSM system, volumetric changes in the presynaptic structures (varicosities) of *Aplysia* live sensory-motor neuron cocultures were observed. The spatial distribution of synaptic vesicle molecules in the preexisting varicosities was monitored together with a volumetric change in the varicosities. Our combined AFM-CLSM system is successfully adapted for measuring learning-related structural changes and the movement of synaptic molecules in the single live neuron through interaction force and fluorescence imaging.



INTRODUCTION

Long-term facilitation (LTF) has been studied as one of the major mechanisms of learning and memory in the *Aplysia* nervous system and is known to be accompanied by functional and structural changes in the synapses between sensory and motor neurons.^{1–4} Spaced or continuous (i.e., massed) application of 5-hydroxytryptamine (5-HT, serotonin) induces LTF.^{5,6} Investigations of LTF with electron microscopy (EM) and optical microscopy revealed that long-term increases in synaptic strength were highly correlated with an increase in the number of functional active varicosities^{2,7,8} and that new varicosities formed from the splitting of the preexisting varicosities of sensory neurons^{1,2,9} or from the outgrowth of new filopodia from the preexisting varicosities of sensory neurons.¹⁰

Optical microscopy and EM have been applied as main methods to study the structural and functional changes in neuronal connections of various species.^{11–15} Optical microscopy generally provides selective and specific visualization of fluorescent markers and makes it possible to monitor dynamic changes in live neurons over time or to visualize the overall shape of the neurons.^{16,17} However, optical fluorescence microscopy has a limitation in obtaining a complete and physiological 3-dimensional (3D) synaptic structure because it only detects optical signals from fluorescence-tagged components. In addition, the spatial resolution of traditional optical microscopy is limited to about half of the wavelength of the light used by the diffraction, and thus the maximum resolution that can be obtained for structural features is only a few hundred nanometers. EM can resolve complex and fine

structures on the nanometer scale and depict 3D structures reconstructed from serial ultrathin sections of samples. EM together with immunohistochemistry has been applied to study the ultrafine structure and function of synaptic connections.^{18–20} However, because EM can only be performed after cell fixation, the observation of the structural changes and movement of functional molecules in live neurons over time is impossible. Thus, a novel tool that can be applied to live cells is necessary to study the functional and structural changes in synaptic connections over time.

Atomic force microscopy (AFM) has nanometer resolution²¹ and has been utilized to investigate the topography of various biosystems such as eukaryotic cells and viruses; intracellular structures such as gap junctions, receptors, and vesicles; and the structural dynamics of these systems under physiological conditions.^{22–28} However, AFM alone is not sufficient to provide a correlation of structural features with functionality. Confocal laser scanning microscopy (CLSM) provides depth-resolved (i.e., z-stacked) in-focus fluorescence images and has been used to trace the 3D dynamics of fluorescence-labeled specific proteins or molecular components within live cells and to clarify intracellular molecular mechanisms.²⁹ Thus, various efforts have recently been made to combine AFM and fluorescent optical microscopy to obtain nanometer-resolution structural and function-specific images of biological phenomena.^{30–36} Several approaches to the combination of AFM and

Received: November 22, 2012

Revised: March 26, 2013

Published: April 5, 2013

CLSM have been reported in the literature, but only the superimposition of 2D fluorescence images onto 3D topography has been applied.^{32,34} The integration of the 3D topography of a live cell with its corresponding 3D fluorescence image has not been reported.

Previous studies on LTF were more focused on the numerical increase in functional varicosities^{2,8} by observing the structural growth of new varicosities from preexisting varicosities. Tracing structural changes in 3D structures of live neurons over time and monitoring spatial distributions of synaptic molecules in live neurons have not been studied mainly because of the limitations of the available imaging techniques for the 3D real-time measurement of nanometer-scale morphological changes in live cells and concurrent 3D imaging of fluorescent molecules in them. Thus, the development of a novel instrument for quantitative analyses of the fine 3D structural changes that occur in the synaptic varicosities during LTF is necessary. In addition, it is important to determine the simultaneous changes in the structures and the 3D localization of intracellular components within the single varicosity during LTF. In the present study, we have developed a combined AFM and CLSM (AFM-CLSM) instrument that provides 3D fluorescent and topographical images at the nanometer scale, and we tried to apply this tool to observe detailed 3D structural changes in synaptic connections and movement of synaptic molecules in live *Aplysia* cultured neurons to confirm its capability of dealing with learning-related synaptic mechanism. We were able to monitor the spatiotemporal changes in the 3D synaptic structures together with the localization of the synaptic vesicle molecules inside those structures by using our developed integration program. After an LTF-inducing stimulus such as continuous (i.e., massed) 5-HT treatment, we observed detailed synaptic connection of *Aplysia* live cultured neurons and a volumetric change in the same preexisting varicosities as well as changes in spatial distribution of synaptic molecules in them. Our tool can be applied to real-time monitoring of in situ structural changes in neuronal structures and simultaneous changes in synaptic functional molecules in them occurring in relation to learning-related mechanism.

MATERIALS AND METHODS

Sensory-to-Motor Neuron Cocultures. To image the cells with the combined AFM and CLSM (AFM-CLSM) instrument, a cell culture dish needs to be modified specifically. The modified culture dish was a standard 60 mm Petri dish of a 35 mm × 30 mm area with a hole drilled from the bottom of the dish. A coverslip was then attached to the bottom of the dish using Sylgard 184 (Dow Corning Corp., Midland, MI). The poly(L-lysine) coating was applied.

Cell cultures were performed as previously described.^{37–39} Abdominal and central ganglia were dissected from *Aplysia kurodai* (50–100 g) and incubated at 34 °C for 1.5–2.5 h in 1% protease (disapse II, 04942078001, Roche Diagnostics Corp., Indianapolis, IN) dissolved in isotonic L15/ASW (1:1) media (L15 medium: Leibovitz, L4386, Sigma-Aldrich, St. Louis, MO; ASW: 460 mM NaCl, 10 mM KCl, 11 mM CaCl₂, 55 mM MgCl₂, and 10 mM HEPES, pH 7.6). After a thorough washing with ASW several times to remove residual protease, the ganglia were incubated at 18 °C for at least 3 h in L15/ASW to allow recovery from heat shock. LFS motor neurons were dissected from the abdominal ganglia and cultured in a solution of 50% *Aplysia* hemolymph in isotonic L15 media. On the next day,

pleural sensory neurons were isolated from the pleural ganglia and cocultured with LFS motor neurons and maintained at 18 °C in an incubator for 3 days to allow time for the formation and stabilization of synaptic connections.

Microinjection of DNA Constructs into *Aplysia* Neurons. Microinjection of DNA constructs into *Aplysia* neurons was performed as previously described.^{40–42} To mark synaptic vesicles-enriched varicosities, sensory neurons in sensory neuron-to-motor neuron cocultures were microinjected with an injection solution containing 0.5 μg/μL of pNEX3-synaptophysin-eGFP (i.e., a plasmid vector containing synaptophysin-eGFP genes for neuronal expression with synaptophysin-enhanced green fluorescent protein) and 0.5 μg/μL of pNEXδ-mRFP (i.e., a plasmid vector containing monomeric red fluorescent protein (mRFP) gene for neuronal expression with red fluorescent protein).

Long-Term Facilitation Protocol. Cultures were exposed to 10 μM 5-HT (5-hydroxytryptamine, serotonin, H7752, Sigma-Aldrich, St. Louis, MO) for 90 min as previously reported.⁵ Control cells were treated with the vehicle (L15/ASW) without 5-HT in an identical manner. To monitor the changes induced by 5-HT treatment, combined AFM-CLSM images of live cells were taken 3 h before 5-HT treatment and 24 h after 90 min of continuous (or massed) 5-HT treatment on them in the bath. To identify the same varicosities, optical images obtained in the same sensory-to-motor neuron coculture were compared before and after 5-HT treatment.

Combined Atomic Force Microscopy and Confocal Laser Scanning Microscopy (Combined AFM-CLSM). The surface structure of fluorescently labeled live cells was investigated with a home-built combined AFM-CLSM system (Figure 1). A MFP-3D (atomic force microscope, Asylum Research) consisted of the AFM head, the AFM X–Y (piezo sample) scanner, and the AFM base. The AFM head and the AFM X–Y scanner were placed on the AFM base. In order to combine the AFM and the CLSM, the MFP-3D was placed on an IX 81 inverted microscope (Olympus, Tokyo, Japan) coupled to a Fluoview FV 1000 confocal laser scanning microscope (CLSM; Olympus, Tokyo, Japan). A fitting stainless steel spacer was inserted between the MFP-3D and the IX 81. When the AFM is combined with the CLSM, there is a chance that a part of the light from a super luminescence diode in the AFM is transmitted through and passes beside the cantilever and so this light can be collected by the objective and it enters the CLSM detector. And thus it may cause a significant background in the fluorescent image.⁴³ To prevent these problems, we inserted an IR cutoff filter (Edmond, NT53-710, Edmund Optics, Barrington, NJ) underneath the objective to block the light in the wavelength of 830–890 nm from the AFM diode. The IX 81 inverted microscope with the AFM head and the AFM scanner installed was placed on a TS-140 antivibration optical table and then this whole unit with an additional confocal scanning unit of Fluoview FV 1000 was enclosed in an acoustically isolated chamber.

In order to get 3D integrated optical and structural images of the same region of the sample, we take the CLSM and AFM images sequentially. After the cantilever is mounted on the AFM head and the light from the AFM diode is aligned on the cantilever, we put the AFM head onto the AFM base with the sample on the XY scanner. The sample and the AFM cantilever positioned near it can be seen through the eyepiece in terms of the illuminating light from the halogen lamp through the CLSM objective lens. The AFM head on the AFM base is

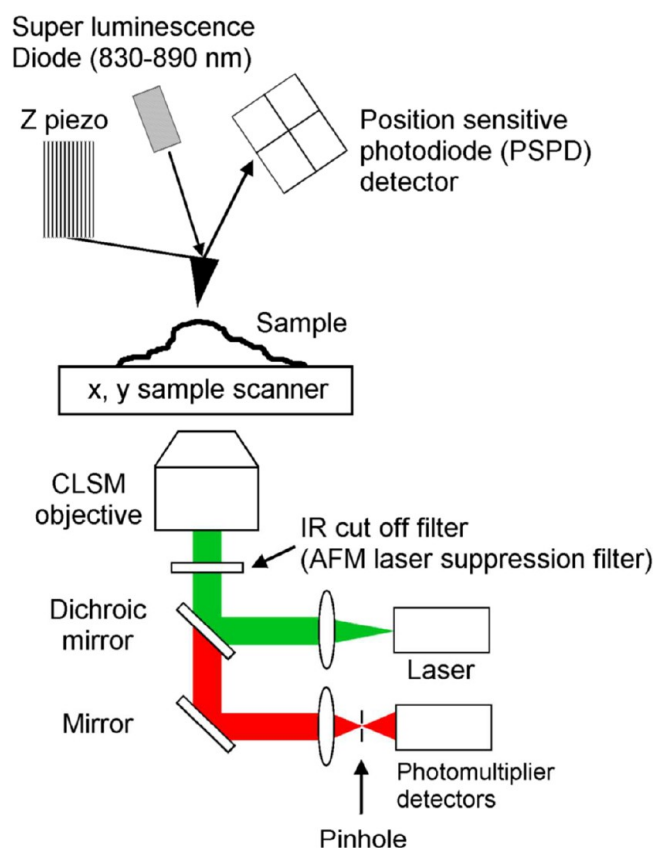


Figure 1. Schematic diagram of the combined atomic force microscope and confocal laser scanning microscope (AFM-CLSM) system.

properly positioned by the adjustment of the AFM base micrometers so that the cantilever on the AFM head lies within the field view of the objective lens of the CLSM unit. In this way, we can locate the AFM tip and optical probe light beam to collect optical and morphological images of the same region of the sample.

The fluorescence images were collected with a 20 \times magnification and an 0.75 NA (numerical aperture) objective lens by the CLSM unit. The fluorescence images from synaptophysin-eGFP and mRFP were obtained by the excitations of a 488 nm blue light from the Ar ion laser and a 543 nm yellowish green light from the HeNe laser, respectively. In order to get a 3D image of live neurons, we collected their depth-resolved (or z-stacked) fluorescence images in every 700 nm. The fluorescence image was recorded at an acquisition rate of 4 ms per pixel. Just right after we took the fluorescent confocal image, we collected the 3D morphological image of the same sample with the AFM unit operating in an AC mode (i.e., a tapping mode) and in liquid. After the alignment of the light from the AFM diode on the cantilever, the AFM-CLSM system was left for half an hour to reach thermal equilibrium. The AFM probe was carefully positioned near the varicosity of a live neuron with the aid of the illuminating light from the halogen lamp which helped us to view the tip so that it did not impale the neuron structure. We conducted an AC (or tapping) mode imaging of the varicosity, using 60 μ m long Biolever cantilevers (Olympus, Tokyo, Japan) with a resonance frequency of 37 kHz in air and a nominal spring constant of 0.03 N/m. The drive frequency for imaging in liquid was set at the nominal resonance frequency of

6–8 kHz. The free-oscillation amplitude of the cantilever was set to 100 nm. The operation amplitude (or set point) was in the range of 70–90% of the free-oscillation amplitude so that the minimal force was applied on the sample. One set of AFM data was composed of 128 scan lines. Each line consisted of 128 data acquisition points. The size of each data acquisition point can be varied and depends on the size of the whole scan area. The scan speed usually was 3 μ m/s for a scan image of 20–30 μ m width. In order to remove inevitable artifacts due to sample tilt, rough surface of glass substrate coated with poly(L-lysine), and etc., the first-order plane flattening was performed using a MFP-3D image processing program.

Data Analysis: Three-Dimensional Integration of AFM Images with CLSM Images.

In order to match the position of the fluorescence-labeled proteins with the corresponding 3D AFM cellular structures, three-dimensional AFM and CLSM images of the same region were integrated by our written program with the aid of MATLAB 7.0.4 (The MathWorks Inc., Natick, MA). When the same sizes of AFM and CLSM images were matched with each other, the text file containing the height information of the structure (i.e., the z-value of every scan point) was created from AFM data; and the other text files containing the fluorescent information of every voxel were created from the fluorescent intensity of each pixel in every focal plane (i.e., each z-value). Our program in terms of MATLAB is written to three-dimensionally match and combine one text file originated from AFM data with the other text file originated from CLSM data. We can also get the 2D cross-section views showing fluorescent signal profiles within the cell's morphology, from the integrated 3D AFM and CLSM image.

Quantification of the Total Number of Varicosities and the Volume of Each Varicosity.

We count the total number of synaptic varicosities labeled with synaptophysin-eGFP in terms of morphological and positional criteria previously established for each sensory neuron.^{2,8,19,44,45} We considered all of the fluorescence-labeled sensory neuron axonal swellings (they have active zones) with a long diameter of greater than 3 μ m in contact with the cell body, the axon hillock, and the proximal segment of axon which were the components of the motor neuron, as functional synaptic varicosities. We measured functional synaptic varicosities in terms of synaptophysin-eGFP fluorescence markers. We collected the overall fluorescent images of SN-MN coculture with low magnification by CLSM and counted the total number of synaptic varicosities. The percentage of change in the number of varicosities was quantified by comparing the total number of sensory neuron varicosities (5-HT-induced newly formed and preexisting) measured at 24 h after 5-HT treatment with those (preexisting) measured at 3 h before 5-HT treatment. 3D fluorescent images of individual varicosities were measured with high magnification to get 3D integrated optical and structural images.

In order to measure the accurate volume of the varicosities, we imaged the 3D structure of the varicosities with the AFM and analyzed the images three-dimensionally as follows. The volume of the synaptic structure was estimated by the sum of all the columns which 3D image was divided into. Each column has a bottom area (typically, 2.4×10^{-14} to 5.5×10^{-14} m²) defined by the pixel and its height corresponding to that of varicosities. Each pixel size is determined by the size of the scan area, the number of scan points per scan line, and the number of scan lines per image. The height values of each column come

from 3D AFM data. The percentage of change in the volume of varicosity was quantified by comparing the volume of a varicosity measured at 24 h after 5-HT treatment with its volume measured at 3 h before 5-HT treatment.⁴⁶ We used six sets of sensory-to-motor neuron cocultures for control experiment and another six sets for 5-HT treatment experiments.

RESULTS AND DISCUSSION

Topography of *Aplysia* Live Neurons Determined by the AFM Unit. We imaged the detailed 3D morphology of subcellular structures in *Aplysia* live sensory neurons by using an AFM in AC mode (Figure 2). Intact morphology and

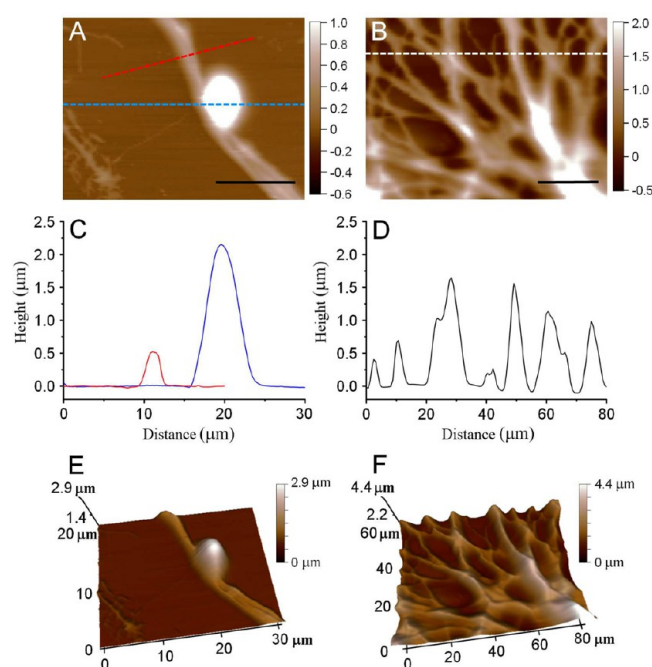


Figure 2. AFM (in AC mode) measurements of *Aplysia* sensory neurons. Two-dimensional height images of (A) a varicosity located in the middle of a neurite, and of (B) multiple neurites. Brown scale bars in (A) and (B) represent the height values in μm . (C) and (D) are the cross-section views along the dashed line shown in (A) and (B), respectively. The varicosity shown in (A) along the blue dotted line has a width of $7.78 \mu\text{m}$ and a height of $2.15 \mu\text{m}$ as clearly seen in terms of the blue solid line in (C). The neurite shown in (A) along the red dotted line has a width of $2.75 \mu\text{m}$ and a height of $0.52 \mu\text{m}$ as seen in terms of the red solid line in (C). The neurites shown in (B) along the white dotted line have a width in the range of $4.50\text{--}9.20 \mu\text{m}$ and a height in the range of $0.46\text{--}1.63 \mu\text{m}$ as shown in (D). (E) and (F) are 3-dimensional (3D) surface reconstructions of the varicosity and neurites shown in (A) and (B), respectively. Scale bars in (A) and (B) are 10 and $20 \mu\text{m}$, respectively.

accurate dimensions of the varicosities and multiple neurites of *Aplysia* sensory neurons were determined on the nanometer scale. The long-axis diameter of the imaged varicosities was varied, ranging from 4.11 to $16.20 \mu\text{m}$, and the height of the varicosities ranged from 1.01 to $3.84 \mu\text{m}$ (the number of varicosities, $m = 10$, chosen to estimate the variation in the diameters and heights). The width of the neurites existing separately from other neurites ranged from 1.66 to $4.96 \mu\text{m}$, and the height of these neurites ranged from 0.35 to $0.84 \mu\text{m}$ ($m = 10$). The synaptic varicosities and neurites, measured in this study, did not reveal particular nanometer-scaled structural

features because *Aplysia* neuronal cell itself was large enough to see and easy to treat when it was measured a whole shape and volume. The scan image size was tens of micrometers for measuring the volume of the varicosities. However, the measured length and height were valid to nanometer scale. If there are the nanometer-sized structural features, the nanometer-scaled features can be observed easily in the scan image size of several hundreds of nanometer. Although the AFM is the most suitable tool for measuring the accurate topography of objects, there are several inherent weaknesses in applying AFM to live cell imaging. First, because of the softness of the live cell membrane, the mechanical force from the AFM tip touching the cell generally depresses the cell membrane and may cause the measured heights to be slightly lower than the actual values.²⁶ Second, because AFM imaging is influenced by the “tip artifact” caused by the convolution between the shapes of the probe and the sample, the width of an object measured with an AFM may be slightly greater than the true width of the sample.⁴⁷ However, when *Aplysia* live neurons were imaged using our AFM with the application of minimal force, the surface of the varicosity and neurites appeared sufficiently hard enough to prevent artificial changes in height. This finding indicates that our AFM imaging technique is suitable for imaging intact structures of *Aplysia* live cultured neurons.

Integrated Images Acquired by the Combined AFM and CLSM System. To determine the neuronal mechanism underlying learning and memory, the correlation between the function and structure of synaptic connections was studied.^{2,48} Learning-related functional and structural changes in synaptic connections were observed in a coculture of *Aplysia* sensory-to-motor neuron synapses.⁴ To understand the detailed mechanism of structural changes, we verified that the custom-built combined AFM-CLSM system can collect the information of structural changes and the localization of intracellular components of the same varicosities. We obtained AFM and CLSM images of the same varicosities in live *Aplysia* sensory neurons cocultured with motor neurons (Figure 3). We integrated AFM and CLSM images to compare them. To distinguish the morphology of the sensory neuron from that of the neighboring motor neuron, sensory neurons were engineered to express the monomeric red fluorescent protein (mRFP). To identify synaptic vesicle-containing varicosities, the sensory neurons were further engineered to express the enhanced green fluorescent protein (eGFP)-tagged synaptophysin (hereafter, synaptophysin-eGFP).² After positioning the cantilever in the field view of the CLSM objective lens, we obtained a 2-channel (i.e., red and green fluorescences) confocal image of sensory neuron varicosities and neurites. To obtain a 3D fluorescence image of these structures, we collected depth-resolved (or z-stacked) fluorescence images every 700 nm . The 3D confocal images from red and green signal channels were projected onto the XY plane to be overlaid on the AFM images. The 2D projected images of the 3D fluorescence images from the red and green signal channels, which were overlapped on the AFM contrast image (Figure 3C) in Figure 3, D and E, are shown in Figure 3, A and B, respectively. The cytoplasm of a sensory neuron was visualized in red by mRFP expression (Figure 3A). The synaptic vesicles tagged with synaptophysin-eGFP were observed to be green within the cytoplasm of the sensory neuron (Figure 3B). We found that the red fluorescence from mRFP expression was relatively evenly dispersed in the varicosity whereas the green fluorescence from synaptophysin-eGFP expression looked

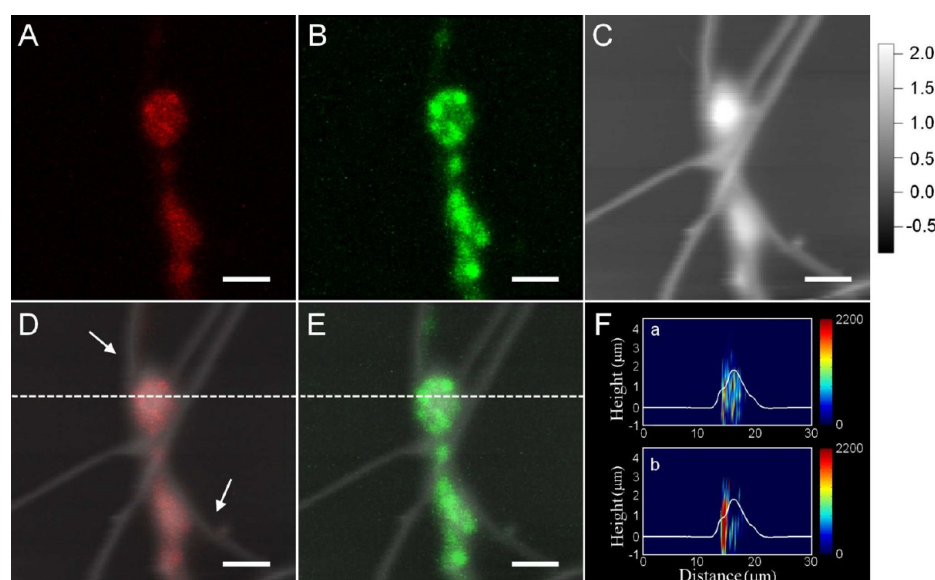


Figure 3. AFM and CLSM images and their overlaid images of the varicosities of sensory neurons in *Aplysia* sensory-to-motor neuron cocultures. Both synaptophysin-enhanced green fluorescent protein (eGFP) and monomeric red fluorescent protein (mRFP) were expressed in the sensory neuron part, which was cocultured with the motor neuron before imaging. (A) and (B) are CLSM fluorescence images. These are 2-dimensional (2D) projected images of 3D CLSM images, which are z-stack collected every 700 nm. The sensory neuron was labeled with both mRFP (A) and synaptophysin-eGFP (B). (C) is a height contrast image obtained by an AFM in AC mode. Gray scale bar represents the height values in μm . (D) and (E) are height contrast AFM images overlaid with 2D projected CLSM images of mRFP (A) and synaptophysin-eGFP (B), respectively. (F-a) and (F-b) are cross-section views (i.e., YZ plane views) of the merged AFM and CLSM (3D) images along the dashed line shown in (D) and (E), respectively. The neurites of the sensory neuron were indicated by two white arrows in (D). The white line (in F) profiles the cell surface and the color scale indicates fluorescence intensity. Scale bars in (A), (B), (C), (D), and (E): 5 μm .

punctuate due to the localization of concentrated vesicles. Because images A and B of Figure 3 were 2D projected images onto XY plane of 3-dimensional CLSM images, one may not clearly see the difference between the red and green fluorescent signals. However, the difference in contrast between red and green signals can be clearly seen in the YZ cross-section images (Figure 3F) rather than the 2D projected images (Figure 3, A and B). After we obtained all of the confocal images, we determined the detailed 3D morphology of the same region by using an AFM in AC mode. The confocal images showed intracellular synaptic components, whereas the AFM images showed the entire surface topography. The topography of the junction region of the sensory and motor neuron coculture is shown with AFM height information provided in different shades of gray (Figure 3C). To merge the AFM and CLSM images properly, the 2D projected CLSM fluorescence images from the red and green signal channels were overlaid on the AFM contrast image (Figure 3, D and E). The region that overlapped with the mRFP fluorescent signal was the sensory neuron, and the other region that did not overlap with the mRFP signal was the motor neuron. However, as shown in Figure 3D, the neurites of the sensory neuron (indicated by two white arrows) did not clearly show red fluorescence (i.e., in CLSM fluorescence imaging). Although the mRFP proteins were expressed evenly throughout the cytoplasm and hinted at the overall morphology of the sensory neurons by their red fluorescence, the optical imaging was not sufficient to reveal fine structures such as neurites labeled with mRFPs because the actual overall shapes obtained by the AFM were not fully recapitulated with the optical imaging. The inability to image fine structures may have also been the result of an insufficient amount of expressed mRFPs for optical detection or the relatively lower optical spatial resolution compared with that of

AFM. Therefore, 3D AFM contrast imaging is essential for the investigation of actual structures. To integrate the AFM and CLSM images, we developed a MATLAB routine (i.e., a short computer program in MATLAB 7.0.4 (The MathWorks Inc.)) that 3-dimensionally matches and integrates AFM and CLSM images of the same region of a sample). The 3D AFM surface plot with height information provided as contrast (i.e., in different shades of gray) was integrated with the 3D CLSM fluorescence image constructed from the z-stacked 2D images (laterally 150 nm, axially 900 nm resolution). The YZ cross-section views of the integrated AFM and CLSM images are shown in panels F-a and F-b of Figure 3 at the dotted line in Figure 3, D and E. The cytoplasmic regions and the positions of synaptic vesicles inside the varicosity were also shown in the 3D morphology of the neuron. Because the lateral resolution (150 nm) of the CLSM is better than its axial resolution (900 nm), the 3D fluorescence images at each point were vertically oval. The cross-section views of the integrated AFM and CLSM images 3-dimensionally revealed that the red fluorescences from mRFPs were relatively evenly dispersed inside the varicosity and the synaptic vesicles tagged with synaptophysin-eGFP were asymmetrically localized in the varicosity (Figure 3F). The accurate sizes of the cellular structures and the intracellular distribution of fluorescent marker-tagged components could be extracted from the AFM and CLSM portions of the 3D integrated CLSM and AFM images, respectively. Our image integration of 3D AFM images with 3D CLSM images is more suitable than simple 2D confocal imaging for the study of synaptic function-related structural changes in *Aplysia* sensory neurons that undergo synaptic plasticity.

5-HT-Induced Changes in the Synaptic Structure and the Localization of Synaptic Vesicle Proteins Analyzed

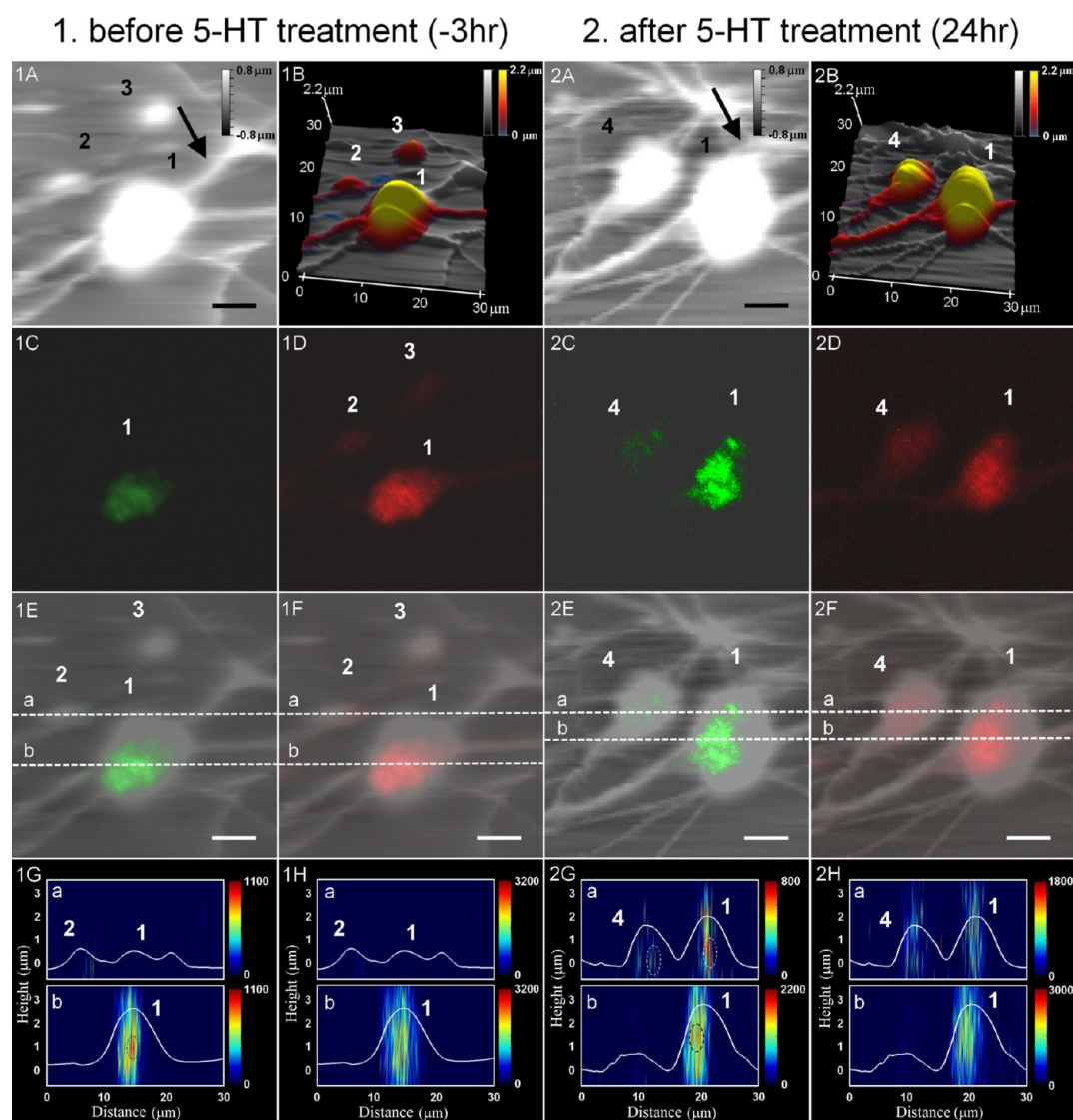


Figure 4. AFM and CLSM images, and their merged images of the presynaptic areas before and after 5-hydroxytryptamine (5-HT) treatment. Images obtained (1) 3 h before 5-HT treatment and (2) 24 h after 5-HT treatment. (1A) and (2A) are height contrast images obtained by AFM. (1B) and (2B) are 3D surface plots of the height images obtained by AFM. Sensory neurons are shown in color. (1C), (1D), (2C), and (2D) are CLSM fluorescence images, and these are 2D projected images of 3D CLSM images that are z-stack collected every 700 nm. The sensory neurons are labeled with both synaptophysin-eGFP (1C and 2C) and mRFP (1D and 2D). (1E), (1F), (2E), and (2F) are height contrast AFM images overlaid with 2D projected CLSM images of synaptophysin-eGFP (1C and 2C) and mRFP (1D and 2D). (1G-a,b), (1H-a,b), (2G-a,b), and (2H-a,b) are cross-section views (i.e., YZ plane views) of the merged AFM and CLSM (3D) images along the dashed line shown in (1E-a,b), (1F-a,b), (2E-a,b), and (2F-a,b), respectively. They show the distribution of synaptophysin-eGFPs and mRFPs within the structure of the synaptic varicosity. The motor neuron, which was not initially labeled with any fluorescent proteins, is indicated by black arrows in (1A) and (2A). The white line profiles the cell surface and the color scale indicates fluorescence intensity. Scale bars in (1A), (2A), (1E), (1F), (2E), and (2F): 5 μm .

by the AFM-CLSM System. We applied the AFM-CLSM system to observe detailed 3D structure of the synapses in live *Aplysia* cocultures. We concurrently monitored spatial distribution of synaptic vesicle proteins in them before and after continuous 5-HT treatment to verify its ability to analyze dynamic changes of synaptic vesicle proteins during LTF. However, we did not directly measure LTF by any electrophysiological means while imaging synaptic structures. We can keep track of the same location unambiguously with a closed loop tracking method. Therefore, we definitely tell what is happening at the same location with an elapse of time. Although we did not measure the sample more often because of being afraid of damaging the single live neuron (not easy to prepare) by the probing laser, we were able to monitor what

was happening at the exact same location during the time evolution with our AFM-CLSM. We were sure to monitor the same area from -3 to 24 h after 5-HT treatment. Thus, we can identify the same varicosities from the optical images of the sensory-to-motor neuron coculture obtained before and after 5-HT treatment. To provide a more accurate correlation between synaptic structural changes induced by 5HT treatment and the localization of synaptic vesicles in the synaptic varicosities, we obtained the AFM and CLSM images of the same synaptic connections before and after 5-HT treatment and analyzed them together. The 3D integrated AFM and CLSM image constructed by our MATLAB routine allowed us to pinpoint the spatial position of the synaptic vesicles within the 3D structures of the synaptic varicosities. We then classified the

varicosities into two different categories in terms of structure: the preexisting varicosities and the newly generated varicosities,² and in terms of intracellular environment: empty varicosities and enriched varicosities. The AFM images provided us with more accurate information on the structures of the sensory neurons and postsynaptic motor neurons that are in synaptic contact with each other. In the optical images obtained by CLSM, a preexisting varicosity (denoted with 1 in Figure 4, 1D and 2D) was observed clearly before and after 5-HT treatment, whereas other preexisting varicosities (denoted with 2, 3 in Figure 4-1D) were not clearly observed before 5-HT treatment, probably because of an undetectable amount of expressed proteins in the relatively small volume of the varicosity. However, the AFM images showed the structure of all the varicosities before and after 5-HT treatment. Before 5-HT treatment, three varicosities (denoted with 1, 2, and 3 in Figure 4-1B) were present as preexisting varicosities, and varicosity 1 was in contact with the major neurites of the motor neuron, which was not initially labeled with any fluorescent proteins (indicated by black arrows in Figure 4, 1A and 2A). After the 5-HT treatment, it is shown in Figure 4-2B that the preexisting varicosity denoted with 1 swelled slightly, and a newly grown varicosity 4 appeared. Optical images further showed the localization of synaptophysin-tagged synaptic vesicles in preexisting varicosities (denoted with 1, 2, and 3) upon 5-HT treatment (in Figure 4, 1C and 2C). The preexisting varicosity (denoted with 1 in Figure 4-1C) filled with synaptic vesicles before 5-HT treatment was kept filled after 5-HT treatment. Preexisting varicosities (denoted with 2 and 3 in Figure 4-1D) was empty before 5-HT treatment, whereas the varicosity 4 (Figure 4, 2C and 2D) was newly grown and became filled after 5-HT treatment. As discussed in Figure 3A, B, Figure 4-1C, -1D, -2C, and -2D are 2D projected images.

The 2D projected images of the 3D CLSM images on the XY plane were overlaid in the AFM height contrast images (denoted in shades of gray) (Figure 4-1E, -1F, -2E, and -2F). The cytoplasmic region of the varicosity (denoted with 1, 2, 3, and 4 in Figure 4, 1F and 2F) visualized by mRFP expression did not cover the overall shape of the varicosity measured by the AFM, possibly because of an insufficient amount of fluorescent proteins for optical detection. As we discussed in Figure 3A, B, 3D AFM contrast imaging is essential to overcome the limitation of optical imaging for the investigation of actual structures. In order to clearly reveal the difference in contrast between red and green fluorescences, the YZ cross-section images are given in Figure 4, 1G, 1H, 2G, and 2H. The YZ cross-section views of the 3D integrated AFM and CLSM images at the dotted lines in Figure 4, 1E, 1F, 2E, and 2F, are shown in Figure 4, 1G, 1H, 2G, and 2H, respectively. The cross-sectional views of the integrated AFM and CLSM images related to 5-HT treatment provided information about the spatial position of synaptic vesicles and cytoplasm that were marked with fluorophores and made it possible to monitor the changes in the position of these sites within the 3D structure of the synaptic varicosity following 5-HT treatment. Because synaptophysin-eGFP is expressed in the membrane of synaptic vesicles, the green fluorescent region indicates the location of synaptic vesicles. The green fluorescent signal from synaptophysin-eGFP appeared to be concentrated at certain regions inside preexisting varicosity 1 before and after 5-HT treatment (Figure 4, 1G-b, 2G-a, and 2G-b, with the regions marked as a dashed oval). The synaptic vesicles were found to be

concentrated at the center of the preexisting varicosity before and after 5-HT treatment. The newly developed varicosity (denoted with 4 in Figure 4-2G-a) was found to be partially filled with synaptic vesicles after 5-HT treatment. Although tracing synaptic vesicles in the varicosity was not possible due to low optical resolution, we were able to observe the 3D localization of synaptic vesicles in the varicosity by monitoring the fluorescence within synaptic connections together with the synaptic morphology of live neurons. Because mRFP was expressed in the entire cytoplasm of the sensory neuron, the red fluorescence from the mRFP was observed throughout the varicosity and was not altered remarkably after 5-HT treatment (Figure 4-1H-b, -2H-b). Our data showed the capability of the combined AFM-CLSM to study learning-related synaptic mechanism. Our tool can monitor the structural changes in synaptic structures of live *Aplysia* sensory neuron-to-motor neuron coculture and the spatial localization and movement of synaptic molecules which can be related to the synaptic function. These results indicate that the integrated AFM-CLSM images can provide an enhanced insight into the spatial position of intracellular components such as synaptic vesicles within live *Aplysia* neurons undergoing LTF. Thus, the combined AFM-CLSM system is an efficient tool for time-course imaging of structural changes and changes in function-related intracellular components in live neurons.

Changes in the morphology of synaptic varicosities have been considered to be an underlying mechanism for the maintenance of synaptic facilitation during LTF. In previous studies, structural changes have been characterized in terms of numerical increase of newly developed varicosities.^{2,9} In this report, we show that our tool provides the information on the accurate volumetric changes in live synaptic varicosities, which may occur during LTF in addition to the numerical increase. The accurate volumetric measurement of preexisting varicosities can provide more detailed information about the correlation between LTF and the structural change in preexisting synaptic structures. Structural changes have been characterized in terms of alterations in the number of synaptic varicosities by 2D optical imaging.^{2,8,49} As mentioned above, although the cytoplasmic region of the cell visualized by the mRFP expression did not cover its overall shape, the volume of the synaptic structure can be approximately quantified by the total fluorescent volume supplemented with an AFM image. By calculating the total red fluorescent volume in the synaptic structure, we estimate the volume of the preexisting varicosities (denoted with 1 in Figure 4, 1D and 2D) before and after 5-HT treatment. The volume of the preexisting varicosity denoted with 1 after 5-HT treatment increased by 35% (from 3.7×10^{-16} to 5.0×10^{-16} m³). With our AFM-CLSM system, the volumetric change in the presynaptic structures can be also accurately measured with AFM. According to our AFM measurements, the volume of the same preexisting varicosity denoted with 1 (in Figure 4, 1B and 2B) increased by 23% (from 1.3×10^{-16} to 1.6×10^{-16} m³) after 5-HT treatment. Although there was a discrepancy between the changes in the varicosity volume measured by CLSM and AFM, the CLSM and AFM both showed an increase in the volume of the synaptic varicosities after 5-HT treatment. The volume measured by AFM is more accurate than that measured by CLSM because AFM has higher spatial resolution than CLSM. The volumetric change in a varicosity measured by the CLSM optical method is known to vary because of the different degree of expression of fluorescent proteins and fluctuating power of

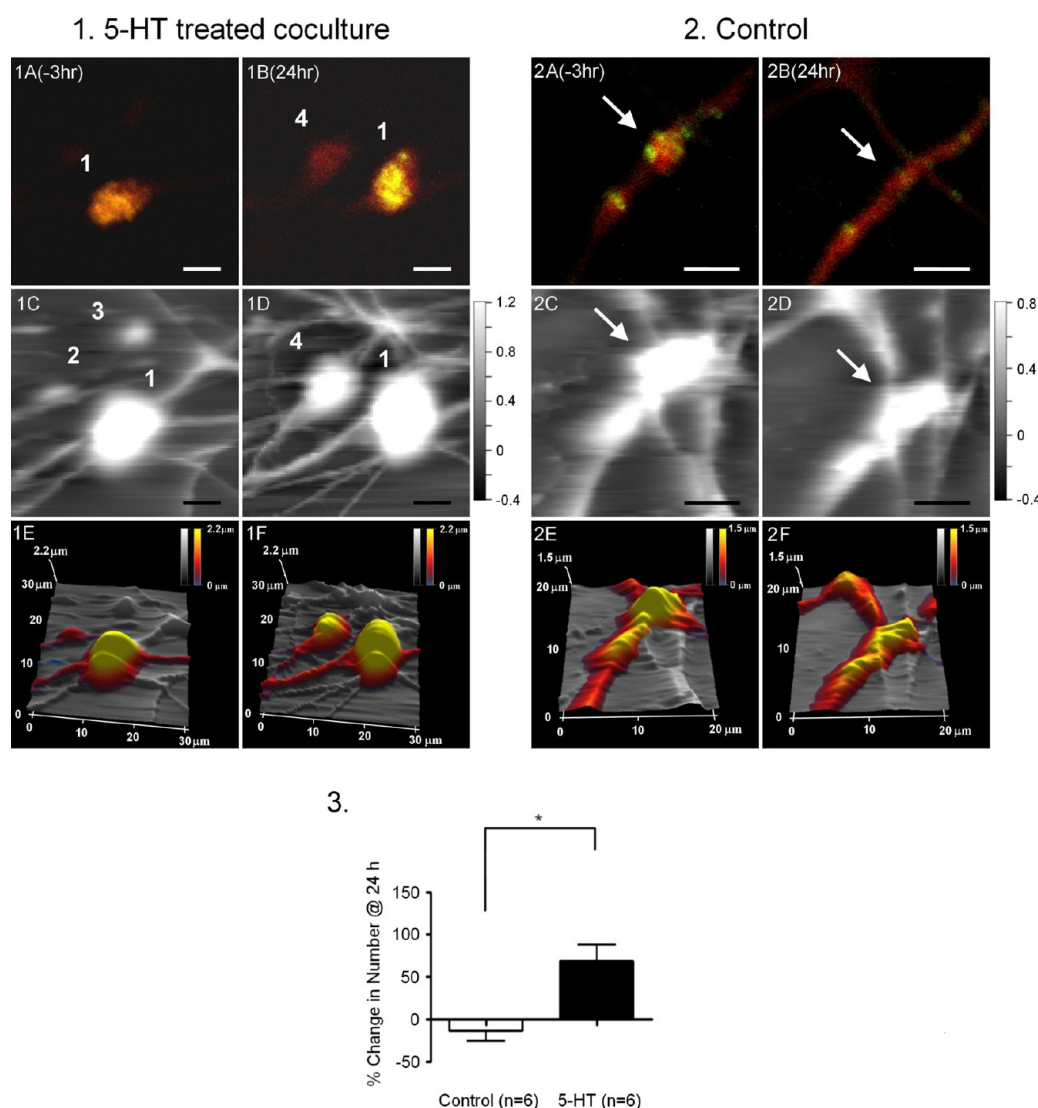


Figure 5. Changes in the volume of synaptic varicosities and/or changes in the total number of synaptic varicosities per coculture induced by 5-HT treatment. Images were obtained from the samples either in the 5-HT-treated condition (1) or in the control condition (2). Both synaptophysin-eGFP and mRFP were expressed in the sensory neuron part, which was cocultured with the motor neuron before imaging. In (1), synaptic varicosities were observed 3 h before 5-HT treatment (1A, 1C, 1E) and 24 h after 5-HT treatment (1B, 1D, 1F). In (2) (control, i.e., no 5-HT treatment), the other synaptic varicosities were observed 3 h before vehicle treatment (2A, 2C, 2E) and 24 h after vehicle treatment (2B, 2D, 2F). (1A), (1B), (2A), and (2B) are 2D merged fluorescence images of mRFP (red) and synaptophysin-eGFP (green) at one focal plane, respectively. They show the distribution of synaptophysin-eGFP within the synaptic varicosities (yellow). (1C), (1D), (2C), and (2D) are morphological changes induced by 5-HT treatment or 5-HT nontreatment, respectively, and are shown with AFM height contrast images. Three-dimensional surface reconstruction images are shown in (1E), (1F), (2E), and (2F), respectively. The shrinkage due to the loss of synaptophysin-eGFP-tagged vesicles is indicated by solid arrows in (2A), (2B), (2C), and (2D). Sensory neurons in sensory-to-motor neuron cocultures are represented by the color scale. The histogram graph (3) shows that the total number of varicosities in the same cocultures used in the analysis of volumetric changes increases after 5-HT treatment ($*p = 0.0044$, unpaired 2-tailed t test). In histogram graph (3), error bars are \pm SEM (standard error of the mean). Scale bars in (1A), (1B), (1C), (1D), (2A), (2B), (2C) and (2D): 5 μ m.

the excitation laser.⁸ Therefore, the volume measurement by AFM is more appropriate for the accurate investigation of volumetric changes in preexisting varicosities than the CLSM optical method. Using the combined AFM-CLSM system, we were able to monitor the structural changes in the synaptic varicosities of live neurons on the nanometer scale.

Analysis of Presynaptic Structural Changes Related to LTF According to Highly Resolved Volumetric Changes.

Previously, the presynaptic change associated with LTF was investigated in terms of changes in the quantitatively measured number of presynaptic varicosities per coculture and in the topological structure, using a conventional optical micro-

scope.^{2,49} Structural changes in synaptophysin-labeled preexisting varicosities, which can be induced by 5-HT treatment, have been seldom studied. We closely observed the changes in preexisting varicosities filled with synaptic vesicles to determine whether there was any volumetric change in addition to the increase in the number of varicosities after 5-HT treatment. To ascertain the effect of 5-HT treatment, we counted the number of synaptic varicosities using the conventional approach (Figure 5-3). The mean number of sensory neuron varicosities in contact with the postsynaptic neuron 24 h after 5-HT treatment was significantly increased ($40 \pm 10\%$, mean \pm standard error of the mean (SEM), $p = 0.0044$, 6 cocultures for

5-HT treated experiments and another 6 cocultures for control, unpaired 2-tailed *t* test), compared with the sensory neuron varicosities in contact with the postsynaptic neuron in control cocultures. This result suggests that our 5-HT treatment was as effective as previous reports, which showed LTF-inducing stimuli increased the number of varicosities in *Aplysia* sensory neuron-to-motor neuron synapses,⁸ even though we did not measure LTF per se by any electrophysiological means. To date, the LTF-related structural changes in synaptic varicosities were mostly measured as alterations in the number of synaptic connections because of the limited capability of the current imaging techniques for live neurons. However, our newly developed AFM-CLSM instrument allowed us to closely and accurately observe the changes in the volume of the synaptic varicosities of live neurons.

We measured the volumetric change and the spatial position of synaptic vesicles in the varicosities of *Aplysia* live neurons by using a combined AFM-CLSM after 5-HT treatment. As shown in Figure 5-1, the 5-HT treatment induced changes in synaptic varicosities. The increase in the number of varicosities filled with synaptic vesicles occurred in the sensory neuron (denoted with 4 in Figure 5). The sensory synaptic varicosity (denoted with 4) developed from the preexisting empty varicosity in contact with the postsynaptic motor neuron and was found to be partially filled with synaptic vesicles. A volume increase in the preexisting varicosity (denoted with 1 in Figure 5) filled with synaptic vesicles was also observed. These volumetric changes in synaptic varicosities have not been shown yet. If synaptic varicosities are labeled with functional synaptic marker such as synapto-pHluorin,⁵⁰ the functional importance of the volumetric changes that we observed can be further identified.

In the previous report, the general life cycle of synaptic varicosities in the coculture (i.e., the formation of new varicosities as well as the maintenance and disappearance of preexisting varicosities) has been reported.⁴⁴ Figure 5-2 shows the disappearance of a preexisting varicosity as part of the life cycle of the synaptic varicosity. Without any 5-HT treatment, the preexisting synaptic varicosity in contact with the motor neuron shrank, and synaptic vesicles marked with synaptophysin-eGFP were lost (this shrinkage is indicated by solid arrows in Figure 5-2). Thus, the drastic change in the volume of the synaptic structure induced by the general life cycle can be studied in depth with our tool. The combined AFM-CLSM system allowed us to precisely analyze the presynaptic structural changes induced by 5-HT treatment by comparing their accurate volumetric data before and after 5-HT treatment. Therefore, this technique helps determine the structural changes that accompany synaptic plasticity on the nanometer scale, with additional chemical information in terms of fluorescence detection.

CONCLUSIONS

Using the combined AFM-CLSM system which allowed us to measure the high-resolution fluorescence and to observe the nanometer-scale structure, we closely evaluated the presynaptic varicosities of a single live neuron. First, the entire 3D image of the overall subcellular structures in *Aplysia* live sensory neurons was acquired by AFM with a nanometer-scale spatial resolution. Second, fluorescently tagged intracellular components were observed through the detection of the optical signal from the same subcellular structures. To determine the correlation between the structure and the intracellular components such as cytoplasm and synaptic vesicles of the synaptic connections, we

integrated their AFM structural and CLSM fluorescent information by our MATLAB program routine.

We were able to image the presynaptic structural changes and changes in the localization of synaptic components in synaptic varicosities after 5-HT treatment. The structural changes in the synaptic varicosities of live neurons were successfully monitored by dynamic AFM over time, which is not possible with EM. Furthermore, changes in the localization of intracellular components of the preexisting varicosities were observed by CLSM fluorescence detection. After 5-HT treatment, there were two types of presynaptic varicosities observed. One type of presynaptic varicosity was synaptophysin-labeled preexisting varicosity, which accompanied volumetric changes (denoted with 1 in Figure 5-1). The other type of presynaptic varicosity was newly developed varicosity from preexisting varicosities and was enriched with synaptic vesicles after 5-HT treatment (denoted with 4 in Figure 5-1). Additionally, the AFM component provides more accurate measurement of the volume of subcellular structures than CLSM, owing to its higher spatial resolution. We report the volumetric change in the varicosities of live neurons by using an AFM for the first time. Without the AFM images (i.e., with the fluorescence image alone), structural change mentioned above could not be clearly determined. With our combined AFM-CLSM installed with a closed loop tracking, we can keep track of varicosities exactly at the same location unambiguously and thus we can monitor what happens at the exact same location during the time evolution. We are sure to monitor the same area before and after 5-HT treatment. Thus, we can clearly identify the volumetric changes induced by 5-HT treatment. Additionally, the mean number of sensory neuron varicosities in contact with the postsynaptic motor neuron 24 h after 5-HT treatment was found to increase significantly ($40 \pm 10\%$, $p = 0.0044$, 6 cocultures for 5-HT-treated experiments and another 6 cocultures for control, unpaired 2-tailed *t* test), which implicated that 5-HT might induce LTF.

Our newly developed AFM-CLSM system is a suitable tool for studying the fine 3D structural changes that occur over time in a single live cell. The functional and morphological changes related to synaptic plasticity can be accurately monitored spatially and temporally by the AFM-CLSM system. In the future, our tool could be applied to real-time monitoring of in situ structural changes occurring in response to external stimuli. This system represents a platform for studying neuronal function and activity as well as neuronal connectivity on a single-neuron level; it could also be used to investigate brain function and activity on the nanometer scale.

AUTHOR INFORMATION

Corresponding Author

*E-mail: shnlee@snu.ac.kr (S.L.); kaang@snu.ac.kr (B.-K.K.). Tel: +82-2-880-1456 (S.L.); +82-2-880-9024 (B.-K.K.). Fax: +82-2-889-1568 (S.L.); +82-2-884-9577 (B.-K.K.).

Notes

The authors declare no competing financial interest.

ACKNOWLEDGMENTS

This work was supported in part by NRF and MOE through BK21 program and the National Creative Research Initiative Program of the Korean Ministry of Science and Technology. We thank KOSEF (for Artificial Atoms Research) and SNU Brain Fusion Program. B.-K.K. and Y.-S.C. were supported by

the National Creative Research Initiative Program of the Korean Ministry of Science and Technology. Y.-S.C. is supported by BK21 fellowships.

REFERENCES

- (1) Bailey, C. H.; Kandel, E. R. *Annu. Rev. Physiol.* **1993**, *55*, 397.
- (2) Kim, J. H.; Udo, H.; Li, H. L.; Youn, T. Y.; Chen, M.; Kandel, E. R.; Bailey, C. H. *Neuron* **2003**, *40*, 151.
- (3) Bailey, C. H.; Kandel, E. R. *Essence of Memory*; Elsevier: Amsterdam, 2008; Vol. 169, p 179.
- (4) Bailey, C. H.; Kandel, E. R.; Si, K. *Neuron* **2004**, *44*, 49.
- (5) Zhang, F.; Endo, S.; Cleary, L. J.; Eskin, A.; Byrne, J. H. *Science* **1997**, *275*, 1318.
- (6) Montarolo, P. G.; Goelet, P.; Castellucci, V. F.; Morgan, J.; Kandel, E. R.; Schacher, S. *Science* **1986**, *234*, 1249.
- (7) Bailey, C. H.; Montarolo, P.; Chen, M.; Kandel, E. R.; Schacher, S. *Neuron* **1992**, *9*, 749.
- (8) Glanzman, D. L.; Kandel, E. R.; Schacher, S. *Science* **1990**, *249*, 799.
- (9) Hatada, Y.; Wu, F.; Sun, Z. Y.; Schacher, S.; Goldberg, D. J. *J. Neurosci.* **2000**, *20*, RC82.
- (10) Udo, H.; Jin, I.; Kim, J. H.; Li, H. L.; Youn, T.; Hawkins, R. D.; Kandel, E. R.; Bailey, C. H. *Neuron* **2005**, *45*, 887.
- (11) Hirokawa, N.; Sobue, K.; Kanda, K.; Harada, A.; Yorifuji, H. *J. Muscle Res. Cell Motility* **1989**, *10*, 270.
- (12) Nimchinsky, E. A.; Sabatini, B. L.; Svoboda, K. *Annu. Rev. Physiol.* **2002**, *64*, 313.
- (13) Sankaranarayanan, S.; Atluri, P. P.; Ryan, T. A. *Nat. Neurosci.* **2003**, *6*, 127.
- (14) Prince, J. S.; Lynn, M. J.; Blackwelder, P. L. *J. Molluscan Stud.* **2006**, *72*, 405.
- (15) Nikonenko, I.; Jourdain, P.; Muller, D. *J. Neurosci.* **2003**, *23*, 8498.
- (16) Hu, X. D.; Viessmann, C.; Nam, S.; Merriam, E.; Dent, E. W. *J. Neurosci.* **2008**, *28*, 13094.
- (17) Gomes, R. A.; Hampton, C.; El-Sabeawy, F.; Sabo, S. L.; McAllister, A. K. *J. Neurosci.* **2006**, *26*, 11487.
- (18) Triller, A.; Rostaing, P.; Korn, H.; Legendre, P. *Neuroscience* **1997**, *80*, 133.
- (19) Bailey, C. H.; Thompson, E. B.; Castellucci, V. F.; Kandel, E. R. *J. Neurocytol.* **1979**, *8*, 415.
- (20) Yamada, K.; Fukaya, M.; Shibata, T.; Kurihara, H.; Tanaka, K.; Inoue, Y.; Watanabe, M. *J. Comp. Neurol.* **2000**, *418*, 106.
- (21) Binnig, G.; Quate, C. F.; Gerber, C. *Phys. Rev. Lett.* **1986**, *56*, 930.
- (22) Hoh, J. H.; Hansma, P. K. *Trends Cell Biol.* **1992**, *2*, 208.
- (23) Ohnesorge, F. M.; Horber, J. K.; Haberle, W.; Czerny, C. P.; Smith, D. P.; Binnig, G. *Biophys. J.* **1997**, *73*, 2183.
- (24) Muller, D. J.; Hand, G. M.; Engel, A.; Sosinsky, G. E. *EMBO J.* **2002**, *21*, 3598.
- (25) Barrera, N. P.; Herbert, P.; Henderson, R. M.; Martin, I. L.; Edwardson, J. M. *Proc. Natl. Acad. Sci. U.S.A.* **2005**, *102*, 12595.
- (26) Xiong, Y.; Lee, A. C.; Suter, D. M.; Lee, G. U. *Biophys. J.* **2009**, *96*, 5060.
- (27) Jena, B. P. *Ultramicroscopy* **2006**, *106*, 663.
- (28) McNally, H. A.; Borgens, R. B. *J. Neurocytol.* **2004**, *33*, 251.
- (29) Pawley, J. B. *Handbook of biological confocal microscopy*, 2nd ed.; Plenum Press: New York, 1995.
- (30) Madl, J.; Rhode, S.; Stangl, H.; Stockinger, H.; Hinterdorfer, P.; Schutz, G. J.; Kada, G. *Ultramicroscopy* **2006**, *106*, 645.
- (31) Lieberman, K.; BenAmi, N.; Lewis, A. *Rev. Sci. Instrum.* **1996**, *67*, 3567.
- (32) Noy, A.; Huser, T. R. *Rev. Sci. Instrum.* **2003**, *74*, 1217.
- (33) Kellermayer, M. S. Z.; Karsai, A.; Kengyel, A.; Nagy, A.; Bianco, P.; Huber, T.; Kulcsar, A.; Niedetzky, C.; Proksch, R.; Grama, L. *Biophys. J.* **2006**, *91*, 2665.
- (34) Kondra, S.; Laishram, J.; Ban, J.; Migliorini, E.; Di Foggia, V.; Lazzarino, M.; Torre, V.; Ruaro, M. E. *J. Neurosci. Methods* **2009**, *177*, 94.
- (35) Gradinaru, C. C.; Martinsson, P.; Aartsma, T. J.; Schmidt, T. *Ultramicroscopy* **2004**, *99*, 235.
- (36) Park, J. W.; Park, A. Y.; Lee, S.; Yu, N. K.; Lee, S. H.; Kaang, B. K. *Bioconj. Chem.* **2010**, *21*, 597.
- (37) Schacher, S.; Proshansky, E. *J. Neurosci.* **1983**, *3*, 2403.
- (38) Lee, J. A.; Kim, H. K.; Kim, K. H.; Han, J. H.; Lee, Y. S.; Lim, C. S.; Chang, D. J.; Kubo, T.; Kaang, B. K. *Learn Mem.* **2001**, *8*, 220.
- (39) Lee, J. A.; Kim, H.; Lee, Y. S.; Kaang, B. K. *Neurosci. Lett.* **2003**, *337*, 9.
- (40) Kaang, B. K. *Mol. Cells* **1996**, *6*, 285.
- (41) Kaang, B. K. *Neurosci. Lett.* **1996**, *221*, 29.
- (42) Kaang, B. K.; Pfaffinger, P. J.; Grant, S. G.; Kandel, E. R.; Furukawa, Y. *Proc. Natl. Acad. Sci. U.S.A.* **1992**, *89*, 1133.
- (43) Kassies, R.; van der Werf, K. O.; Lenferink, A.; Hunter, C. N.; Olsen, J. D.; Subramaniam, V.; Otto, C. *J. Microsc.* **2005**, *217*, 109.
- (44) Miniaci, M. C.; Kim, J. H.; Puthanveetil, S. V.; Si, K.; Zhu, H.; Kandel, E. R.; Bailey, C. H. *Neuron* **2008**, *59*, 1024.
- (45) Glanzman, D. L.; Kandel, E. R.; Schacher, S. *Neuron* **1989**, *3*, 441.
- (46) Schneider, S. W.; Pagel, P.; Rotsch, C.; Danker, T.; Oberleithner, H.; Radmacher, M.; Schwab, A. *Pflugers Arch.* **2000**, *439*, 297.
- (47) Eaton, P.; West, P. *Atomic force microscopy*; Oxford University Press Inc: New York, 2010.
- (48) Hawkins, R. D.; Kandel, E. R.; Bailey, C. H. *Biol. Bull.* **2006**, *210*, 174.
- (49) Bailey, C. H.; Chen, M. *Proc. Natl. Acad. Sci. U.S.A.* **1988**, *85*, 2373.
- (50) Sankaranarayanan, S.; De Angelis, D.; Rothman, J. E.; Ryan, T. A. *Biophys. J.* **2000**, *79*, 2199.